Electronic Supplementary Material (ESI) for Nanoscale.

Uncovering thermally activated purple-to-blue luminescence in Co-modified MgAl-layered double hydroxide

Bianca R. Gevers [*a,b], Emil Roduner [c,d], Andreas Leuteritz[b] and Frederick J.W.J Labuschagné[a]

* Corresponding author: bianca.gevers@tuks.co.za

[a] *Department of Chemical Engineering, Institute of Applied Materials, University of Pretoria, 0002 Pretoria, South Africa.*

[b] *Leibniz-Institut für Polymerforschung Dresden e.V., Institute of Polymer Materials; Processing Technology, D-01069 Dresden, Germany.*

[c] *Department of Chemistry, University of Pretoria, 0002 Pretoria, South Africa.*

[d] *Institute of Physical Chemistry, Universität Stuttgart, D-70569 Stuttgart, Germany.*

S1 Synthesis

The nano-sandrose layered double hydroxides (LDHs) were prepared using co-precipitation at a constant pH of 11 [1,2] with a molar M^{II+}/M^{III+} ratio of 2:1. To obtain the Co-modified LDHs, Mg was substituted with Co at molar concentrations of 0.5 %, 1 %, 5 %, 10 %, 25 %, 50 %, 75 % and 100 %.

To synthesise the compounds, chemically pure (CP) or analytical grade (AR) reactants were used. $AlCl_3 \cdot 6H_2O$ (CP), $MgCl_2 \cdot 6H_2O$ (AR), $CoCl_2 \cdot 6H_2O$ (AR), NaOH (AR) and Na_2CO_3 (AR) were sourced from ACE Chemicals. De-ionised water was used throughout.

The precipitation was carried out by drop-wise addition of a salt solution containing Mg-, Al-, and Co-ions in with a total metal-ion concentration of 2.56 M and a base solution of 10 M NaOH into a 0.4 M Na_2CO_3 solution under vigorous stirring. The precipitate formed was filtered off using vacuum filtration and the crystals were washed with 5 l of water. The washed crystals were dried at 60 °C for 18 h and ground to a fine powder prior to analysis.

S2 Material properties

S2.1 X-ray diffraction patterns

X-ray powder diffraction (XRD) measurements were performed on a Panalytical X'Pert PRO X-ray diffractometer in $\theta - \theta$ configuration, equipped with Fe-filtered Co-Kα radiation (1.789 Å) and an X'Celerator detector and variable-divergence- and fixed receiving slits. Samples were prepared according to the standardised Panalytical backloading system, which facilitates the nearly random distribution of the particles. Data were collected in the angular range $5° \leq 2\theta \leq 80°$, with a step size of 0.008° 2θ and a 13 s scan step time. The phases were identified using X'Pert HighScore Plus software. The spectra were converted from variable slit to fixed slit prior to phase identification. The detection limit for the crystalline phases was 2 %. The XRD patterns of the MgCoAl-LDHs are shown in Figure S1. No crystalline impurities were detected apart from an insignificant calcite peak (not detectable by eye) in MgCoAl-2.

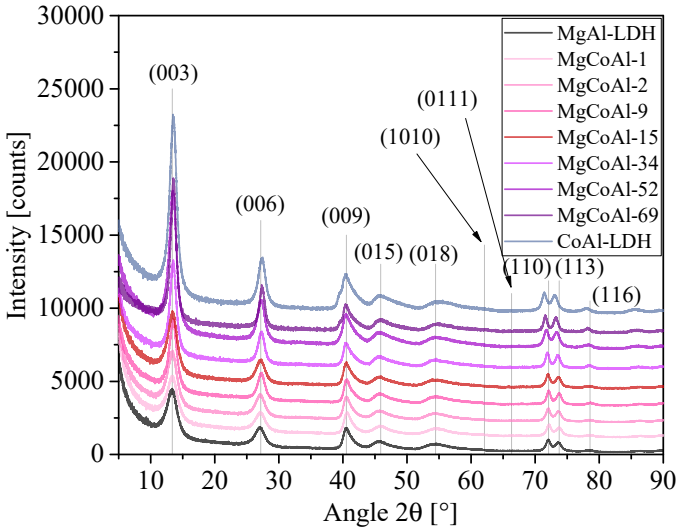

Figure S1 XRD patterns for the MgCoAl-LDHs with a Co-content of 0.5 %, 1 %, 5 %, 10 %, 25 %, 50 %, 75 % and 100 %.

S2.2 Scanning electron microscopy micrographs

SEM images were taken with a Zeiss Gemini Ultra Plus FEG SEM, and a Zeiss Gemini 2 Crossbeam 540 FEG SEM. The samples were prepared by evenly distributing the samples on carbon tape on an aluminium stub and coating it with two layers of carbon (angles: 0°, -45° and +45°) using a sputter coater. The micrographs were taken at 1 keV. The SEM micrographs of the LDHs are shown in Figure S2.

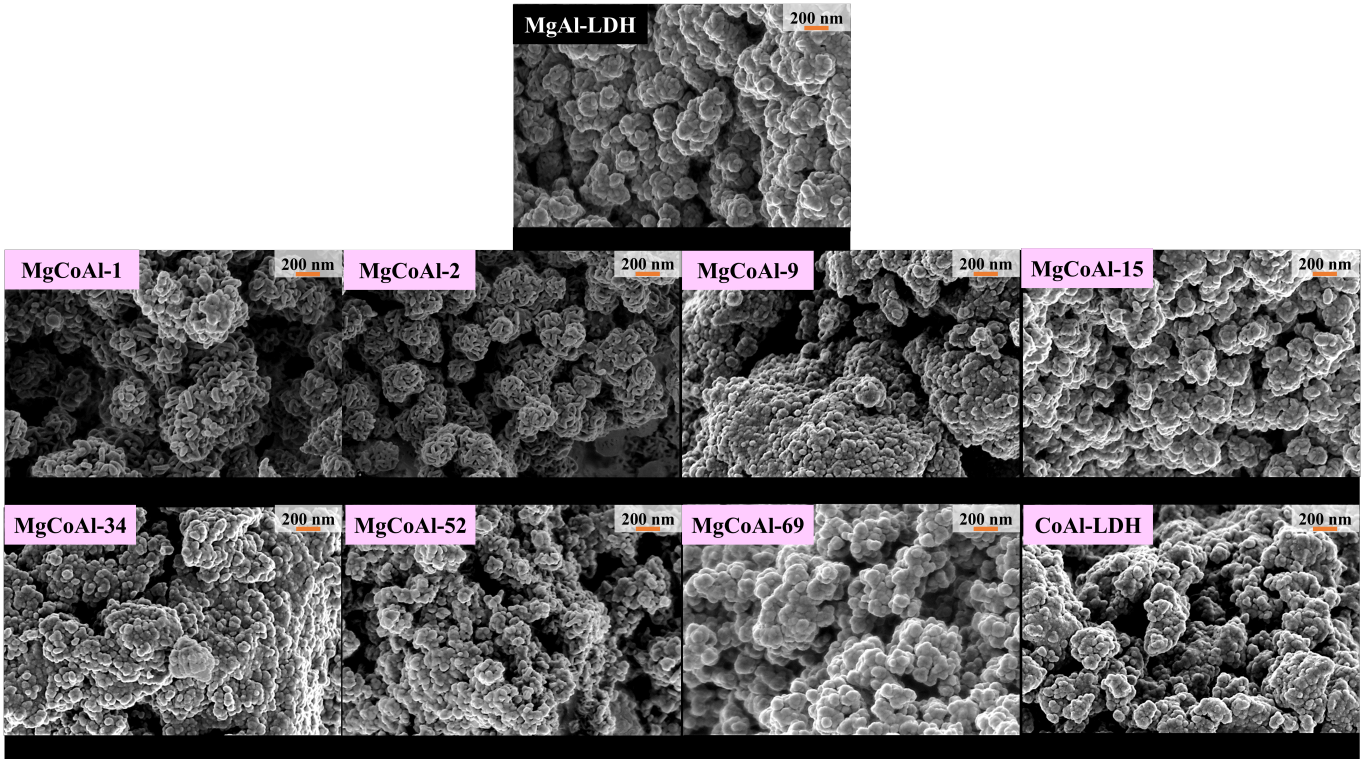

Figure S2 SEM micrographs for the MgCoAl-LDHs with a Co-content of 0.5 %, 1 %, 5 %, 10 %, 25 %, 50 %, 75 % and 100 %.

An SE2-filtered micrograph of MgAl-LDH (Figure S3), was taken on a Zeiss Ultra Plus and shows the sandrose-like structure of the LDHs in more detail. The sample was distributed on a stub and coated with 3 nm of platinum using a sputter coater. The micrograph was taken at 3 keV with the SE2 filter in place.

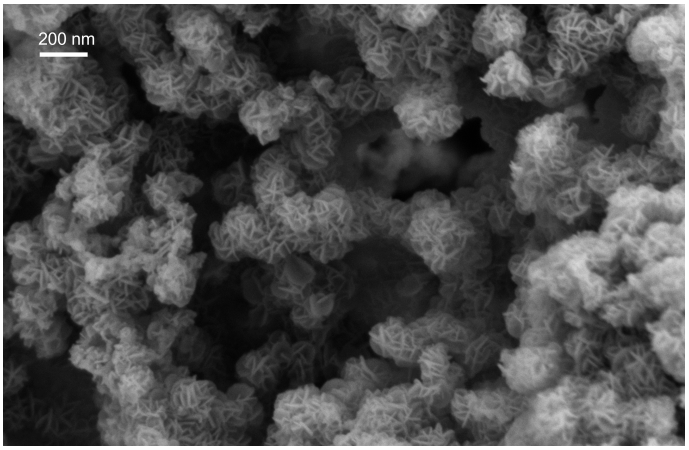

Figure S3 SE2 filtered scanning electron micrograph showing the nano-sandrose structure of MgAl-LDH obtained at 3.0 keV[1].

S2.3 Inductively coupled plasma optical emission spectroscopy

Inductively coupled plasma optical emission spectroscopy (ICP-OES) was used to verify the elemental ratio of Mg:Al:TM in the MgMAl-11 LDHs and identify impurities in the materials. The ICP-OES results are depicted in Figure S4 and show that the Co ion was preferentially integrated into the LDH structure, leading to higher concentrations of Co.

The Co content for the samples was found to be 1, 2, 9, 15, 34, 52, 69, and 82 mol% of the cations in the LDH structure, leading to a Mg-for-Co replacement percentage of 1, 3, 13, 22, 47, 68, 86, and 100 % instead of the desired 0.5, 1, 5, 10, 25, 50,

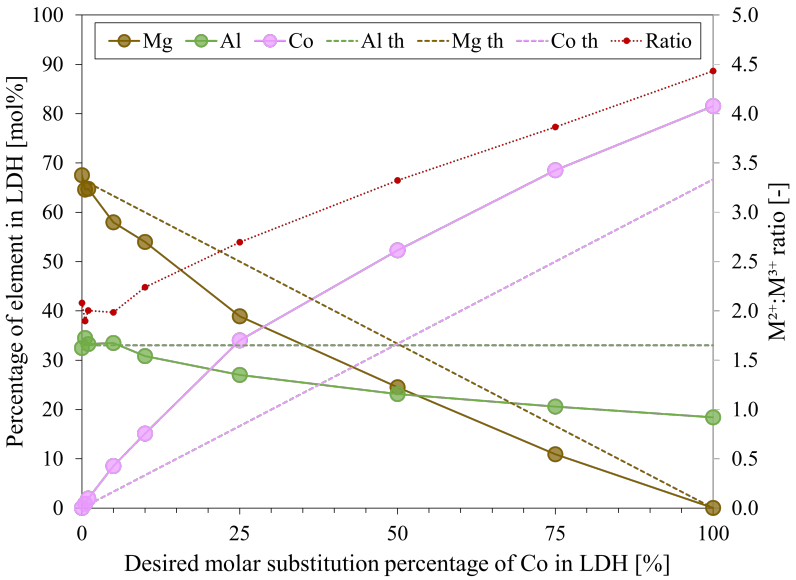

Figure S4 Composition of the MgCoAl-LDHs with a theoretical Co-content of 0.5 %, 1 %, 5 %, 10 %, 25 %, 50 %, 75 % and 100 %, showing the actual molar percentages of Mg, Al and Co *versus* the theoretically desired percentages and the M^{II+}/M^{III+} metal ratio under the assumption that Co is included only in its divalent form. [1]

75 and 100 %. The preferential inclusion of Co into the LDH structure is common, and seen across synthesis methods [2,3], even with the use of methods, which provide highly accurate elemental ratios for other transition metals [1,2]. Figure S4 shows that, under the assumption of Co^{2+}-inclusion only, the M^{II+}/M^{III+} would significantly exceed the desired 2:1 ratio. The colour of the samples obtained disagrees with a high M^{II+}/M^{III+} ratio [4] and strengthens the argument of Co^{3+} inclusion as validated on the optical spectra of the LDHs (see Figure 2a). If the Co accommodated for all Mg and Al lost, a M^{II+}/M^{III+}-ratio range between 2.0 and 2.6 would be achieved, agreeing also with the colour of the samples in comparison to those of higher M^{II+}/M^{III+} ratios [4]. The colours of the materials are shown in Figure S5.

Figure S5 Colours of the series MgAl-LDH, MgCoAl-LDHs and CoAl-LDH with a Co-content of 0, 1, 2, 9, 15, 34, 52, 69, and 82 mol%.

S3 Optical properties

S3.1 Bandgaps

To obtain the bandgaps using the Tauc plot method, the d-d transitions (band with an edge at 2.22-2.24 eV) were excluded from the analysis as they present a different excitation mechanism to the one required for band traversal from the CB into the VB. The Tauc plots of the LDH spectra show multiple features, corresponding to the broad bands of the absorption spectra visible above 3 eV. For the band edge, the lowest determinable tangent-cross-value after the d-d transition region was identified as the start of the CB. Figure S6 shows the bandgap analysis results of the MgCoAl-LDHs. The bandgap narrows from 3.18 eV (MgAl-LDH) to 3.17 eV, 3.2 eV, 3.0 eV, 3.44 eV, 3.0 eV, 2.95 eV, 2.82 eV and 2.86 eV (CoAl-LDH) with an increase in Co-content. MgCoAl-22 shows a clear deviation from the narrowing trend, which region overlaps with the thermally-activated luminescence band.

S3.2 Luminescence repeatability

Photoluminescence spectra were recorded on a Deep UV miniPL 5.0 between 260 nm and 650 nm with a stepsize of 2 nm and using an excitation wavelength of 248 nm (spot size 70 μm). Data were transformed from wavelength- to energy-dependence using the formula $I(E) = I(\lambda) \times \lambda^2$. [5] Temperature-dependent spectra of each material were obtained using the same sample and the same spot of excitation to ensure the best possible comparability. The measurement was started at 83 K, followed by 200 K and ended with 298 K.

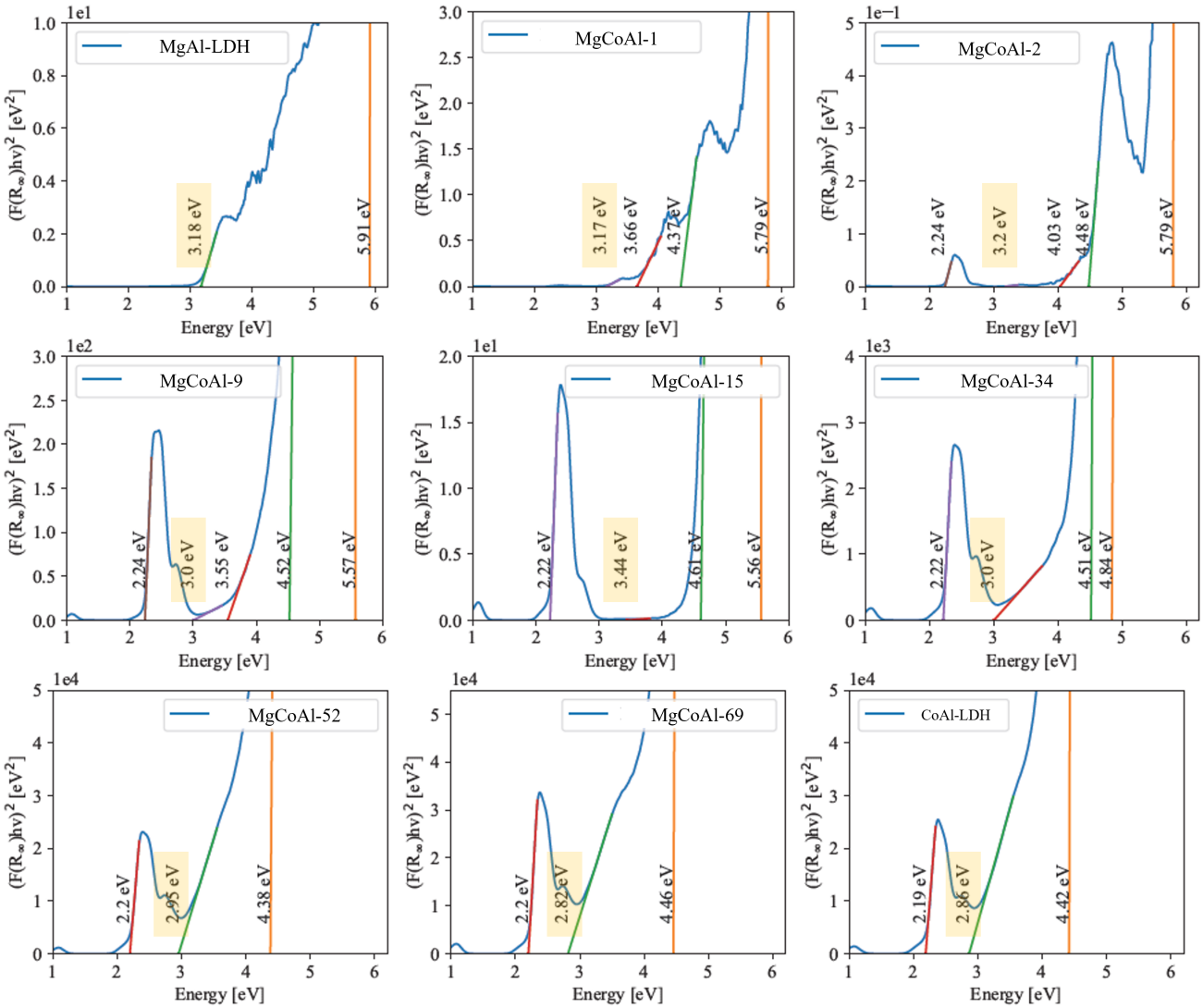

Figure S6 Graphical band edges of the MgCoAl-LDHs obtained through use of the Tauc plot method with r = 0.5 (direct allowed transitions) for the absorption spectra shown in Figure 1. Modified from [1].

Figure S7 shows the luminescence repeatability results of MgCoAl-10. To obtain these luminescence spectra, a different spot on the same sample was studied. The thermally-activated luminescence band at 298 K is repeatable in its intensity and position. At the lower temperatures, the band does not luminesce as strongly. This may reflect an inhomogeneity in the sample composition.

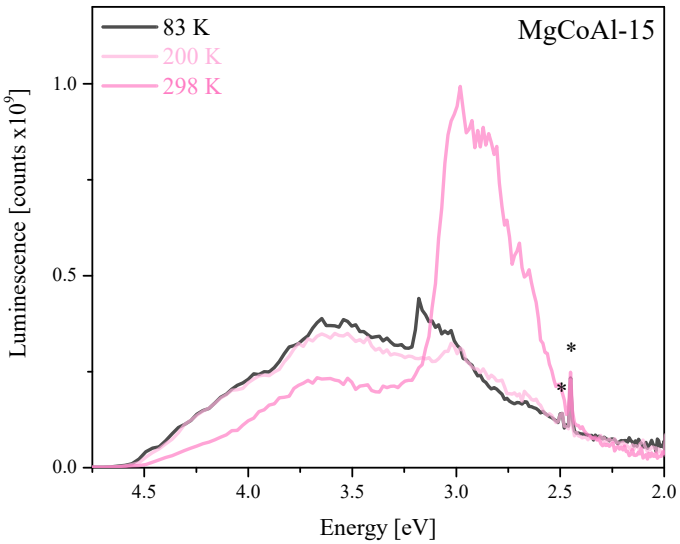

Figure S7 Repeatability experiment of the luminescence of MgCoAl-15 at 83 K, 200 K and 298 K.

References

[1] B. R. Gevers, *The effects of transition-metal modification on MgMAl-layered double hydroxides for use in photofunctional applications*, 2023.

[2] B. R. Gevers, S. Naseem, A. Leuteritz and F. J. Labuschagné, *RSC Advances*, 2019, **9**, 28262–28275.

[3] S. Naseem, B. Gevers, R. Boldt, F. J. Labuschagné and A. Leuteritz, *RSC Advances*, 2019, **9**, 3030–3040.

[4] R. D. S. Macedo, R. Boni Fazzi, A. M. Da Costa Ferreira and V. R. L. Constantino, *New Journal of Chemistry*, 2020, **44**, 10022–10032.

[5] I. Pelant and J. Valenta, *Luminescence Spectroscopy of Semiconductors*, Oxford University Press, Oxford, 2012, p. 542.